

Article

Mechanical Behaviour of a Metal-CFRP-Hybrid Structure and Its Components under Quasi-Static and Dynamic Load at Elevated Temperature

Hendrik Jost ^{1,*}, Felix Grossmann ²  and Hans-Georg Herrmann ^{1,3} ¹ Chair for Lightweight Systems, Saarland University, Campus E3 1, 66123 Saarbrücken, Germany² Institute for Manufacturing Technology and Production Systems, TU Kaiserslautern, Gottlieb-Daimler-Str., 67663 Kaiserslautern, Germany³ Fraunhofer Institute for Nondestructive Testing IZFP, Campus E3 1, 66123 Saarbrücken, Germany

* Correspondence: hendrik.jost@izfp-extern.fraunhofer.de; Tel.: +49-681-9302-3930

Abstract: Hybrid materials containing a light metal and CFRP are capable to make a relevant contribution in lightweight design and thereby in reducing greenhouse gases causing global warming. An aluminium CFRP-hybrid specimen with a thermoplastic interlayer that is suitable for application for the A-, B-, or C-pillar in a car is investigated in this work regarding the mechanical behaviour due to temperature variation. For this purpose, quasi-static as well as dynamic tensile tests are carried out not only for those hybrid specimens but also for their respective single-material components. Those are supported by various non-destructive testing (NDT) techniques such as thermography and CT-scans of X-ray tomography. The examination of the single materials as well as the hybrid specimens gives us the possibility to understand if a change in the damage process of the hybrid is caused by one of the single materials or the interaction of them. The use of the NDT techniques in combination with the mechanical experiments allows us to obtain a deeper look at the mechanisms causing the respective damage. It stands out that temperature changes affect the damage mechanisms in the hybrid significantly without having great influence on the single materials. In quasistatic testing, the maximum displacement of the hybrid specimens rises at elevated temperature, and in dynamic testing the initial stiffness and the sustained cycles decline significantly. It therefore can be concluded that the interfaces inside the hybrids are affected by temperature changes and play a major role concerning the damage mechanisms. The pure knowledge about the temperature behaviour of single materials is not sufficient for anticipating the behaviour of hybrid specimens under these restrictions.

Keywords: NDT; thermography; CFRP; hybrid; quasi-static testing; dynamical testing; X-ray tomography; temperature variation; interfaces



Citation: Jost, H.; Grossmann, F.; Herrmann, H.-G. Mechanical Behaviour of a Metal-CFRP-Hybrid Structure and Its Components under Quasi-Static and Dynamic Load at Elevated Temperature. *Appl. Sci.* **2022**, *12*, 12824. <https://doi.org/10.3390/app122412824>

Academic Editor: Jaime Batista dos Santos

Received: 14 November 2022

Accepted: 8 December 2022

Published: 14 December 2022

Publisher's Note: MDPI stays neutral with regard to jurisdictional claims in published maps and institutional affiliations.



Copyright: © 2022 by the authors. Licensee MDPI, Basel, Switzerland. This article is an open access article distributed under the terms and conditions of the Creative Commons Attribution (CC BY) license (<https://creativecommons.org/licenses/by/4.0/>).

1. Introduction

Due to the global warming caused by greenhouse gases such as carbon dioxide, there is a common consent in society, politics, and the industry that the emission of those gases has to be reduced. There are different approaches in the automotive industry to reach this goal. One of them is the increase of the proportion of electric and hybrid electric vehicles or fuel cell cars. Another approach is the technological optimisation of combustion cars. All those approaches have in common that lightweight design is a key part of them [1]. Carbon Fibre Reinforced Polymers (CFRP) already plays an important role for lightweight in aircraft or in the sports car industry due to outstanding specific mechanical properties. Since CFRP still is too expensive to be used for the complete body-in white, multi-material design is used as a cost-optimized lightweight concept [2], which requires a joining technology of CFRP to metals that is suitable for large-scale production. Such an approach is the intrinsic metal-CFRP-hybrid of investigation, which is discussed in [3–7] as well. This hybrid

specimen consists of a three-armed aluminium inlay overmoulded with polyphthalamide (PPA-GF30) that is interlock-laminated in CFRP (see Figure 1).

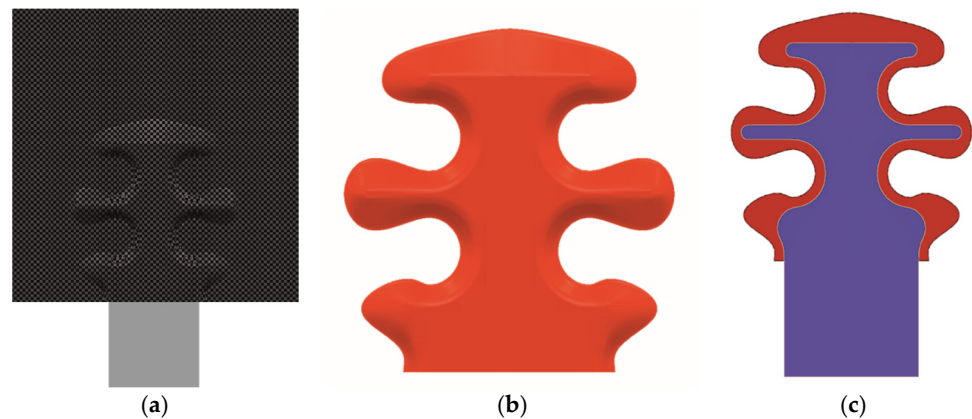


Figure 1. Illustrations of (a) the hybrid (b) the PPA-GF30 overmoulded insert and (c) the aluminium insert.

The good mechanical performance of such a hybrid specimen under laboratory conditions in quasi-static and dynamic tension testing is shown in [3,6]. To be worth considering in automotive application it is furthermore important to show a robust material behaviour under different weather conditions such as heat, frost, or rain. On top of that, the damage mechanisms of the hybrid specimen and the temperature influence have to be understood: Regarding the complex geometry of this type of hybrid and considering it consists of three different materials connected by two interfaces, there is a challenge in extrapolating from the behaviour of the single materials to the behaviour of the hybrid specimen. There already is a lot of research regarding the temperature influence of polymers, CFRP or adhesive bonds. The novelty of the here-presented research lies in the complexity of the intrinsic hybrid specimen itself and an improvement of understanding how small changes in the behaviour of the single materials can lead to significant changes in the hybrid specimen.

To meet those challenges, different fields of research should be considered, i.e., intrinsic metal–CFRP hybrids and the mechanical behaviour of the used materials at elevated temperatures.

1.1. Intrinsic Metal–CFRP-Hybrids

Due to the growing importance of metal–CFRP hybrids, a lot of different approaches can be found in literature. One is the use of pin structures on the metal surface, which penetrate the fibre fabric before the infusion and cure of the resin [8]. This leads to a big improvement of the mechanical properties, while the manufacturing effort is too high for serial production. Another approach is “laser direct joining” of CFRP to metal [9]. A strong physical bonding can be achieved, but the method is limited to thermoplastic matrix materials.

An upcoming new concept is based on the intrinsic hybridisation. The general concept as well as different approaches are discussed in [10]. Intrinsic hybridisation means that the manufacturing of the hybrid takes place in one process step [10,11], which makes it suitable for serial production and allows the use of thermoplastic as well as thermosetting polymers. For the manufacturing of intrinsic metal–CFRP hybrids, different processes are suitable. In [12], rotational moulding is used to produce shaft connections while in [13], automated fibre placement (AFP) is used to build up multilayer inserts.

The specimens investigated in this work are manufactured in a resin transfer moulding (RTM) process and are a geometrical optimisation of the specimens that are discussed in [3–6]. The characteristic of this approach is the thermoplastic interlayer (PPA-GF30), which prevents contact corrosion and lowers the stiffness gap between aluminium and CFRP leading to enhanced mechanical fatigue properties [3]. This generates two different interfaces that should be considered in further observations.

1.2. Mechanical Behaviour at Elevated Temperatures

An understanding of the temperature behaviour of the represented metal–CFRP hybrids and its components is of utmost importance. In experiments, the mechanical behaviour at the temperature levels of 23 °C and 60 °C is investigated. Hence, in the following chapter, the temperature behaviour of aluminium, CFRP, and PPA-GF30 is shortly described regarding current literature with focus on this temperature range.

Aluminium as a metal exhibits a naturally higher temperature resistance than the PPA-GF30 or the epoxy matrix of the CFRP. The crystalline structure of metals allows much higher temperatures without deforming or degrading the material. Up until 100 °C, the predominant mechanism of plastic deformation is dislocation gliding. The mechanical properties, whilst static testing, do not change significantly until 100 °C. The melting point for unalloyed aluminium lies at 660 °C, whereas the properties in dynamical testing are not examined as much [14].

Since most common matrix materials are thermosets and thermoplastics, the role of the matrix becomes more important when testing CFRP at higher temperatures. For this research, a thermosetting epoxy resin matrix was used. Since thermal and mechanical properties of a polymer rely heavily on process parameters and underlying monomers, this results in a wide range of different polymers which can consist of similar structures. In conclusion, even comparisons in the same polymer class (i.e., epoxy) are difficult to obtain, but compared to the melting point of carbon fibres or aluminium, the epoxy resin softens and finally decomposes at a relatively low temperature.

Cao et al. [15] carried out tests on the mechanical behaviour of CFRP at elevated temperatures using rectangularly shaped specimens. A dropdown of the tensile strength to about 68% at 60 °C was observed when 100% is at 16 °C, but eventually remaining constant at this level. This leads to the assumption that once the glass transition temperature (T_g) of the matrix is exceeded, it contributes less to the tensile strength, hence lowering the tensile strength of the CFRP. This is implied by a comparison of dry carbon fibres which only reach 48% of the tensile strength of the CFRP at 16 °C. He also detected a change of failure modes for CFRP above 120 °C [15].

Im et al. [16] performed three-point bending tests and focused on the influence of temperature changes on the flexural strength and the delaminated area of CFRP with two different matrix types (epoxy and PEEK). It turned out that the delamination area of the CF/EPOXY specimens increased inversely proportional to the surface temperature. Conclusive to that, lower temperatures exhibit larger delamination areas [16].

The tensile fatigue life prediction of CFRP was investigated by Miyano et al. [17]. They showed that with given stress ratio, frequency, and temperature the tensile fatigue life can be predicted by obtaining a master curve. This prediction method works for satin-woven CFRP laminates as well as unidirectional CFRP [17].

The term PPA-GF30 refers to a fibre reinforced polyphthalamide (PPA). In this case, it is filled with 30 vol.% of cut glass fibres. Generally speaking, the mechanical behaviour of polymers is strongly dependent on temperature, loading frequency and strain rate. Additionally, the tensile strength and stiffness of polymers are much lower than those are for aluminium. In this case, only thermoplastics and thermosets are considered. Thermoplastics melt before decomposing, whereas thermosets just decompose. The polyphthalamides contain an aromatic as well as an aliphatic group, which stabilise them at high temperatures. The heat distortion temperature of this PPA-GF30 with 290 °C is very high compared to other common used polymers [18].

Lyons [19,20] compared the mechanical behaviour of different PPA and polyamide (PA) types after isothermal ageing. He showed the degradation of the secant modulus as well as the tensile strength for PPA and PA at higher temperatures. He concluded that PPA is superior to PA in terms of tensile strength, creep-rupture life, and stiffness when it comes to high temperature applications especially in the long run [19]. Furthermore, the standard failure mechanisms, which are fibre fracture with matrix crack and fibre pull-out, were not affected by the temperature change but the degree of their contribution to failure. On top of

that, SEM observations unveiled a dependence of matrix ductility and fibre pull-out length to the surface roughness in creep-rupture tests [20].

L. Ke et al. [21] investigated how the fatigue performance of previously damaged steel specimens can be influenced by CFRP patches and further investigated the influence of testing temperature. The main findings were that the CFRP patches effectively can enhance the fatigue performance of the specimens and that the elevated temperature (60 °C) weakens the fatigue performance of the created steel–CFRP specimens significantly. They further describe premature debonding for some specimens at 60 °C and a shift in debonding mechanisms from CFRP/adhesive layer debonding at lower temperatures to adhesive layer/steel debonding at elevated temperature levels (>45 °C).

Y. Chen et al. [22] investigated the temperature influence of a hybrid bonded–riveted joint connecting CFRP and aluminium. It could be seen that joint strength and energy absorption is temperature-dependent, and it could be observed that higher temperature led to a more severe failure of the CFRP substrate around the rivet hole.

D. Mrzljak et al. [23] developed a fatigue testing procedure for steel–CFRP hybrids with a special look at self-healing effects. They furthermore used simulations to investigate the influence of thermal residual stress (TRS) due to elevated temperatures and stated that an influence of the TRS cannot be neglected.

1.3. Research Significance

Although the above-mentioned results show similarities to those in this paper, experiments at elevated temperatures with such a material combination and such a complex geometry cannot be found in the literature. There is some research in the mechanical behaviour of metal–CFRP hybrids with two different materials and a simple geometry (mostly single or double lap joints) regarding only the mechanical data. The significance of the here-conducted work lies in the consideration of a more complex geometry and material combination and the involvement of NDT techniques to obtain further information about the underlying damage mechanisms. The exact behaviour of the CFRP hybrids under these conditions cannot be predicted, and further investigation is needed.

2. Materials and Methods

The hybrid specimen as well as the single-material specimens are mechanically tested under two different temperature conditions and examined with non-destructive testing methods (in situ passive thermography and X-ray projections). This way, the damage mechanisms can be observed, and it can be assigned if the damage occurs in the bulk material or on the surface.

2.1. Examined Specimens

As explained above, the hybrid specimen (see Figure 2, right) consists of four plies plain weave carbon fibre laminate, which is arranged in a $[0/90, \pm 45]_s$ layup. The fibres used are T300/FT300 from TORAY [24] with a biresin CR170/CH150-3 from Sika [25]. Between the middle layers of the CFRP an inlay of the aluminium alloy AlMgSi1 (EN AW 6082-T6 from “Schmolz + Bickenbach”) [26] is located. The aluminium inlay itself is enclosed by the thermoplastic PPA-GF30 via direct injection-moulding (“VESTAMID® HTplus M1033” from Evonik Industries AG, Essen, Germany) [27]. The hybrid specimen is manufactured in an RTM process by draping the overmoulded metal inlay between the middle carbon fibre layers. The thickness of the CFRP plate is 1 mm. It must be mentioned that the manufacturing of these specimens is prototypical and carried out manually. Despite a good care of cleanliness, even small defilement can lead to debonding and affect the mechanical behaviour. Furthermore, short differences in curing time during the RTM process affect the glass transition temperature of the epoxy and thus the mechanical properties.

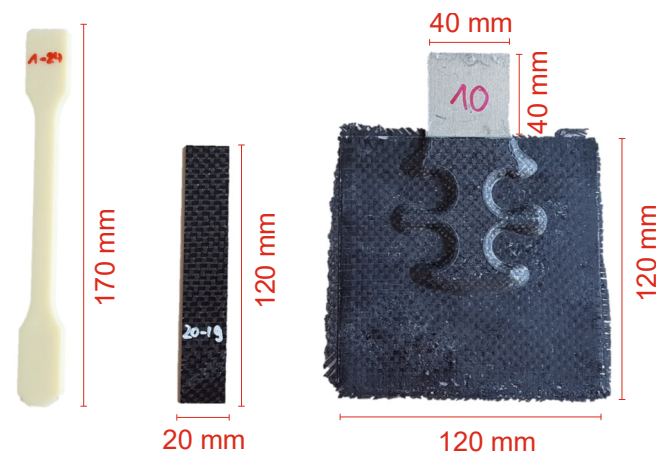


Figure 2. Left: dog bone PPA-GF30 specimen; middle: flat tensile CFRP specimen; right: assembled hybrid specimen.

The flat tensile specimen of CFRP (see Figure 2, middle) consists of the same textile and resin as the hybrid and is produced in an RTM process with a thickness of 1 mm as well. The specimen shape is inspired by DIN EN ISO 527-4 (type 2) [28] with a downscaling to one half due to a better comparability to the hybrid specimens.

On the left-hand side of Figure 2, a dog bone tensile specimen of PPA-GF30 is depicted that is manufactured in an injection moulding process with a thickness of 4 mm and a web width of 10 mm. The shape is appropriate to the norm 527-2 (type 1A) [29].

The mechanical parameters of the used materials are summarized in Table 1.

Table 1. Mechanical data of the materials extracted from their data sheets [24,26,27].

	Young's Modulus [GPa]	Tensile Strength [MPa]	Elongation at Break [%]
PPA-GF30	11	160	1.7
Carbon fiber	230	3530	1.5
aluminium	67	310	10

The glass transition temperature of PPA-GF30 is 290 °C, while its melting point is 308 °C. Due to the large-scale production process of the CFRP and hybrid specimens, the cure time is relatively short. On the basis of the data sheet the glass transition temperature of the epoxy at the given parameters (20 min cure time, 80 °C and 8 bar) is between 60 °C and 80 °C [25].

2.2. Thermography

Non-destructive testing (NDT) includes several methods—for example, eddy current, ultrasonic testing, or thermography. The latter is a well-known method for CFRP testing. One main advantage of this method is contactless testing of large areas in a really short amount of time. For the problems arising with this hybrid specimen, thermography as NDT method is most suitable. First, this is because the specimen is installed in the tensile testing machine and not easily accessible for mechanical contact, thus contactless testing comes in handy. Second, large areas can be tested in a short period of time. Third, the resulting temperature difference especially for CFRP is high (see Equation (1) [30]):

$$\Delta T_{diss}(t) = \frac{Q_{diss}(t)}{\rho c_p} \quad (1)$$

where ΔT_{diss} is the temperature difference induced by the dissipated heat quantity Q_{diss} , density ρ , and the specific heat capacity c_p . CFRP exhibits a relatively low density and

a medium specific heat capacity, which increases ΔT , considering the largest and most important area of the hybrid specimen consists of CFRP. Thermography relies on infrared (IR) irradiation, which is emitted by objects above zero Kelvin according to Planck's Law:

$$L_{\lambda,b} = \frac{2hc_0^2}{\lambda^5 \left[\exp\left(\frac{hc}{\lambda KT}\right) - 1 \right]} \quad (2)$$

Planck's Law describes the emittance of the spectral radiance L by a blackbody dependent on wavelength λ and temperature T . The spectral radiance L is a parameter measured by the thermography camera, which is then converted to a temperature. Therefore, the emissivity ε also plays an important role when a temperature value is assigned to a value of L . Equation (2) only applies to black objects, but under real circumstances spectral radiance also depends on the solid angle ω , radiant power ϕ , the angle between centre line of the radiation cone, and the sphere normal θ as well as the surface increment dA from which the electromagnetic waves are emitted:

$$(\lambda, \theta, \phi) = \frac{d^3\phi}{dA \cos\theta d\omega d\lambda} \quad (3)$$

Emissivity ε now relates the spectral radiance L_λ of a specimen to the spectral radiance of a blackbody $L_{\lambda,b}$ [31,32]:

$$\varepsilon(\lambda, T, \theta, \Phi) = \frac{L_\lambda(\lambda, T, \theta, \Phi)}{L_{\lambda,b}(\lambda, T)} \quad (4)$$

In consequence to that, ε is also dependent on all of these parameters which makes it very difficult to measure. For a precise quantitative measurement of the temperature, the emissivity must be known. The contrast in thermography images comes from different temperature, surface properties, emissivity, or material type besides the temperature distribution of the surface. Additionally, porosities can be the origin of an inhomogeneous distribution or an apparent higher temperature. Furthermore, mechanical loading can alter the temperature of a specimen. Under tensile loading a specimen will expand and thus lower its temperature vice-versa for compression. Sometimes it is more beneficial for thermographic measurements to build temperature differences. In most cases, emissivity can then be neglected [31].

For thermography, there are 2 typical wavelength segments. The first one is called mid-wavelength infrared (MWIR). It reaches from about 3 to 8 μm . The second one is the long wavelength infrared (LWIR) from 8 to 15 μm . These measurements here are performed with a camera sensitive to the atmospheric window (LWIR).

Thermography is divided into a passive and an active branch. Passive thermography uses only the infrared waves emitted from the specimen without putting extra energy into it. By measuring the radiated heat waves, thermography methods can assign a temperature to it. Additionally, those measurements are mostly of qualitative nature. Therefore, it is common to build the temperature difference to a reference state of the specimen (i.e., before testing). The resulting ΔT -images show temperature differences compared to the unloaded state. In addition to that phase or amplitude, images can be acquired via Lock-In thermography. Active thermography relies on external energy input via heat sources such as flash lamps, ultrasound emitters, or a radiant heater. The thermal stimulation of the specimen raises its temperature and may interfere with subsurface flaws. According to the different temperature decay into the bulk material, the user is able to detect porosities, impurities or near surface anomalies in the thermograms [31].

2.3. Thermoelastic Effect

The behaviour of a material exhibiting the thermoelastic effect under sinusoidal load and adiabatic conditions can be described as follows:

$$\Delta T_{el}(t) = -\frac{T_0 \alpha \sigma_a}{\rho c_p} \sin(2\pi f t) \quad (5)$$

This formula relates the elastic temperature change ΔT_{el} to the starting temperature T_0 , the coefficient of thermal expansion α , the applied stress σ_a , the density ρ , the specific heat under constant pressure c_p , as well as the time t and the modulation frequency f . It can be seen that a positive tensile load results in a negative elastic temperature change and vice-versa. The mechanical loading will lead to a temperature change, which can be detected by the IR camera. For CFRP, the density is relatively low, and the coefficient of thermal expansion is high which yields in a high ΔT_{el} . Therefore, CFRP presumably shows a good contrast in a thermoelastic analysis [30].

2.4. Lock-in Thermography

As a part of the active thermography branch, there is a very surface-sensitive technique thermography method called Lock-In thermography. It can extract useful extra information from dynamical tests. The material is periodically thermally excited by an external source with modulation frequency f . This source can be the same as before mentioned for active thermography as long as it can be modulated periodically. The phase difference of the exciting source and the thermally induced heatwaves detected by an infrared camera can be used to detect flaws beneath the surface, whereas the information depth is inversely proportional to the modulation frequency. These phase differences are displayed in a phase picture. Besides that, there is also an amplitude picture which captures the amplitude of the periodically varying surface temperature. Those are more suitable for estimating the severity of the damage, whereas phase pictures are more sensitive to slight changes even with low amplitude. The advantage of the periodical excitement with a sine wave is a reduced evaluation time for each averaged Lock-in image because the sine can be reconstructed with a minimum number of four points [31,33].

In this paper, thermography with mechanically induced energy input via quasi-static and dynamical tensile loading was used as well as lock-in thermography.

2.5. X-ray Microtomography

X-ray computed tomography in general is an established method that is used in medicine, industry, and science. The well-known basic principle is the irradiation of an object with X-rays from different angles and the reconstruction of these projections to a 3D image or a 2D slice image [34]. A contrast occurs due to the highly material dependent attenuation of X-ray photons according to the law of Lambert–Beer [34]. In material science and non-destructive testing, the microstructure is of particular interest, and therefore resolutions in the micrometre range are required. This task can be fulfilled by the X-ray microtomography (μ -CT).

The μ -CT is a Procon X-ray CT-alpha with an X-ray source of 30–160 kV. The resolution of the detector is 2304×2304 pixels leading to a pixel size of 50 μm . The pictures showed in this paper are 2D projections.

2.6. Experimental Set-Up

The experimental set-up used in this study is an Instron 8500 tensile testing machine with 100 kN loading cell connected to a computer, which controls the recording parameters of the mechanical and thermographic data. The hybrid specimen is fixated in a U-shaped clamping as presented in Figure 3, while the tensile specimens are fixated in clamping jaws. The thermography images are recorded by the VarioCAM[®] HD head from InfraTec (InfraTec GmbH, Dresden, Germany) [35]. It detects electromagnetic waves in the LWIR

range (7.5–14 μm) with a resolution of 1024×768 pixels and a sensitivity (noise equivalent thermal detectability) of 50 mK using a microbolometer-array [35].

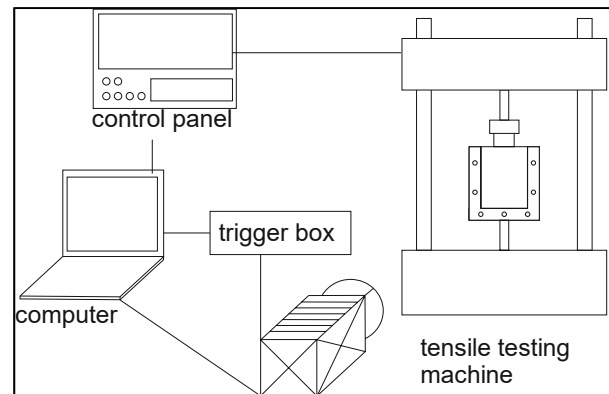


Figure 3. Scheme of the experimental set-up.

At the start of any mechanical test, the computer triggers the infrared (IR) camera to take pictures.

As testing procedures for all specimen types, quasi-static tensile testing as well as dynamical testing are chosen. The quasi-static experiments are carried out displacement-controlled with a crosshead speed of 2 mm/min inspired by DIN EN ISO 527 [28,29]. These are continuously recorded by the thermography camera with 3 frames per second (fps).

The dynamical experiments are executed force-controlled in the tension area with $R = 0.1$ and with 75% of the maximum force at 23 °C, which the examined specimen type can tolerate in quasi-static testing. These experiments are recorded non-continuously with thermography. The times at which the camera records an image package is based on the number of load cycles. The camera receives a total of 11 signals for cycles 1, 100, 200, 300, to 1000. A trigger-signal is then sent every 5000 loading cycles. An image package contains 18 images and is recorded at a frequency of 30 Hz.

3. Results

3.1. Quasi-Static Testing

The complex geometry of the hybrid specimen does not allow the calculation of stress and strain. Therefore, in Figure 4a, the force-displacement diagram of two exemplary PPA-GF30 specimens can be seen at 23 °C and 60 °C, respectively. Comparing those two curves, both the slope and the maximum force are lower at 60 °C than at 23 °C. Both curves are rising steadily with a decreasing slope and show a typical behaviour for brittle polymers due to their viscoelastic properties. Furthermore, the displacement at rupture is slightly higher at 60 °C. An explanation is that polymers generally become softer the nearer they get to their glass transition temperature. The same observations can be made for the curves of the CFRP, and the same explanation as for PPA-GF30 could be applied to the CFRP specimens (see Figure 4b) because of their polymer epoxy matrix. The behaviour of the hybrid specimens is depicted in Figure 4c. For 23 °C, a dropdown in force occurs in rather short and drastic events, whereas at 60 °C, a smoother curve can be seen. As an explanation, different damage mechanisms in the hybrid specimen depending on the test temperature can be suggested. Displacement is significantly higher and also the area under the graph is bigger at 60 °C, which implies a higher energy absorption. Due to the generic specimen geometry, it was not possible to find a visual criterion when a specimen failed. Therefore, a threshold of 10% of the maximum force of the hybrid specimens was defined as failure criterion.

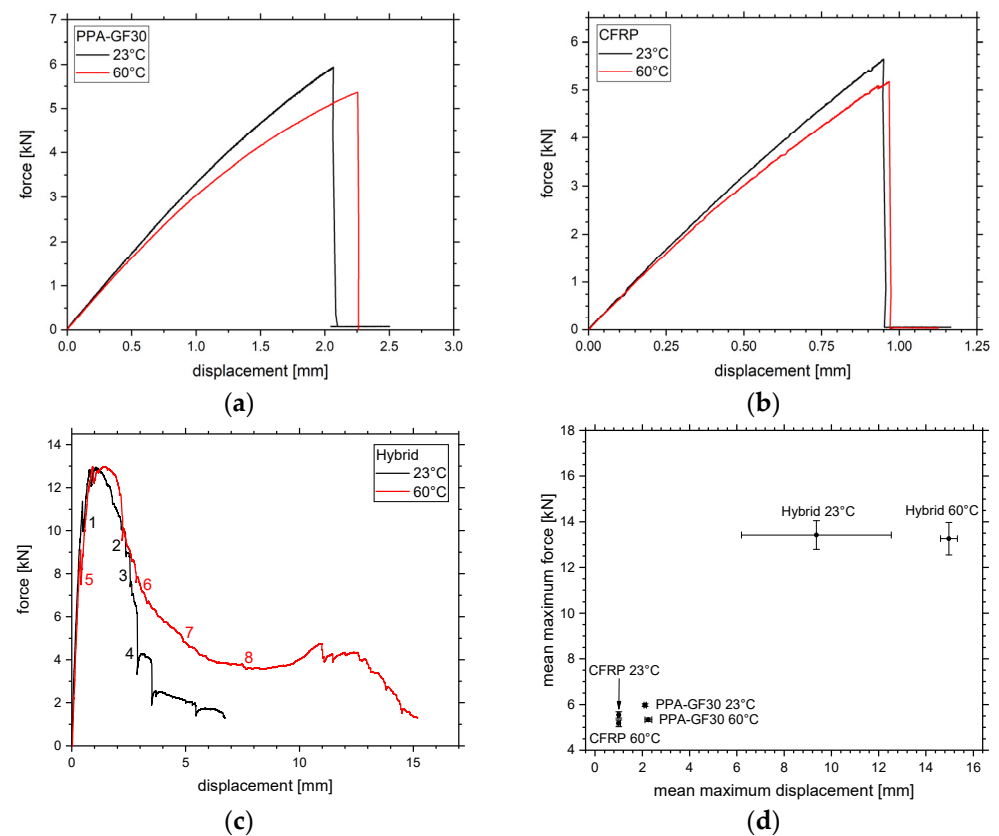


Figure 4. Force-displacement curves of (a) PPA-GF30, (b) CFRP, (c) hybrid specimen, and (d) mean maximum values of force over displacement (very small error bars for PPA-GF30 and CFRP). For the hybrid, maximum displacement is reached if $F < 0.1 F_{max}$.

The increase in displacement at failure for the three shown force-displacement diagrams in Figure 4a–c leads to the assumption that the polymers, i.e., the PPA-GF30 and the epoxy matrix, soften at 60 °C. To verify these assumptions, the mean values of multiple equal specimens with their according error bars (standard deviation) are pictured in Figure 4d. Comparing them shows that this can only be verified for the hybrid specimens, which show a significant increase in maximum displacement. For PPA-GF30, the increase in displacement is slight but the CFRP specimens show no evident difference. However, the mean maximum force decreases from 23 °C towards 60 °C for PPA-GF30 and CFRP. This also contributes to the hypothesis of the softening. In Table 2, a brief comparative analysis is given for the PPA-GF30 and CFRP specimens at 23 °C and at 60 °C to emphasise those results. Due to the big error bars, there is no such comparison for the hybrid specimens. Error bars for PPA-GF30 and CFRP are very small, which shows that there is a high reproducibility.

Table 2. Comparative analysis of PPA-GF30 and CFRP specimens at the two different testing temperatures.

Specimen Type	Mean Maximum Displacement [mm]		Percentage Variance [%]	Mean Maximum Force [kN]		Percentage Variance [%]
	23 °C	60 °C		23 °C	60 °C	
PPA-GF30	2.11 ± 0.04	2.25 ± 0.11	6.2	5.97 ± 0.04	5.33 ± 0.06	12
CFRP	1.00 ± 0.38	1.00 ± 0.06	0	5.55 ± 0.11	5.17 ± 0.13	6.8

To obtain further information about the differences in damage mechanisms, a closer look is taken at the thermograms of the PPA-GF30 and the CFRP specimens. The thermograms in Figure 5 show the specimens right after cracking. The images are depicted in ΔT

contrast, which means that the first thermogram is subtracted from each of the following thermograms. In conclusion, a difference in the surface temperature distribution can be seen as contrast. At failure, the crack can be observed as a rectangular-shaped heat flash by the thermography camera. The emission of heat at 23 °C (see Figure 5a left specimen) lies at about 3–4 °C, which is about the same for 60 °C (see Figure 5a right specimen). Comparing all the PPA-GF30 specimens, it can be concluded that no temperature differences at the crack can be measured between 23 and 60 °C.

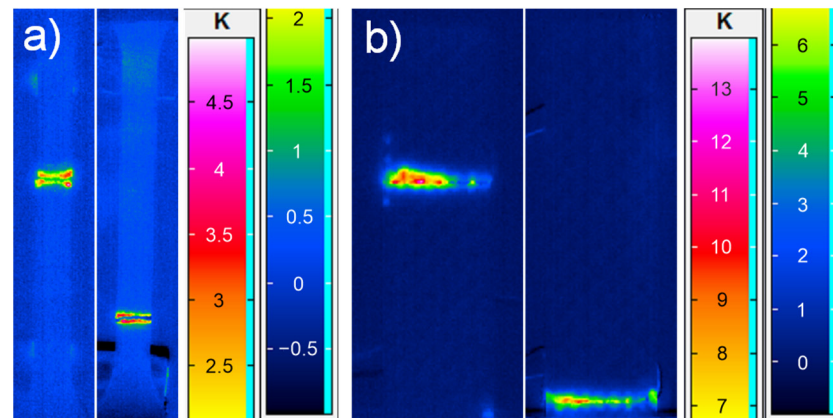


Figure 5. ΔT -thermograms of (a) the PPA-GF30 specimens at 23 °C (left) and 60 °C (right) and (b) the CFRP specimens 23 °C (left) and 60 °C (right) in quasi-static testing.

The heating of the CFRP specimens seen in Figure 5b is up to 11 °C, thus higher than the heating of the PPA-GF30 specimens. There is also no evidence that the heat released by the crack is vastly different for 23 °C and 60 °C in CFRP.

In situ thermography on the hybrid specimens is represented in Figure 6. The thermograms 1–8 show the hybrid at specific damaging events during the tests. Note that the white and black dotted lines indicate the position of the insert. In the first four images the thermograms of the quasi-static test at 23 °C are depicted.

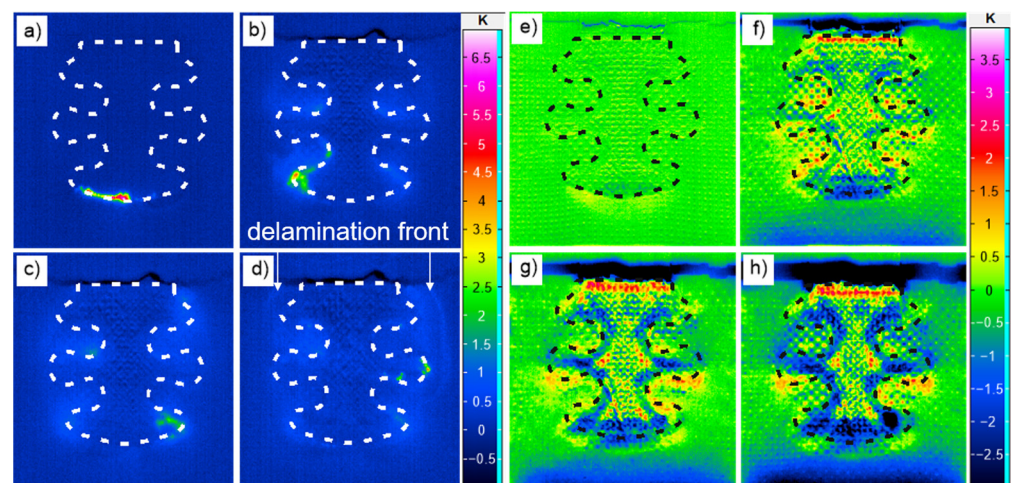


Figure 6. ΔT -thermograms of the hybrid specimens at 23 °C (a–d) and 60 °C (e–h) in quasi-static testing.

Picture 1 in Figure 6 shows clearly visible damage, resulting in a crack directly below the aluminium insert. The temperature rises up to 5.5 °C at the crack, which lies right in between the values for PPA-GF30 and CFRP. Initial damage in form of cracking or delamination below the insert can be observed for all hybrid specimens. Afterwards, more delaminations and cracks arise (green contrast in pictures 2–3) until most of the area around the insert is damaged. Those delaminations and cracks raise the temperature by 2–5 °C. In

picture 4 (see Figure 6), a light blue contrast (@ $T = 1\text{ }^{\circ}\text{C}$) on the right side around the insert shows the final delamination. This encloses the damaged area of the hybrid specimen. Ultimately, the delamination leads to an opening of the CFRP “bag”, and the insert gets pulled out of it.

For the tests at $60\text{ }^{\circ}\text{C}$, the first delamination also starts below the insert (see picture 5 in Figure 6) without cracking. Thereafter, the contrast between insert and CFRP laminate increases as delaminations come up (see picture 6 in Figure 6). This also happens at $23\text{ }^{\circ}\text{C}$ but with a much lower contrast, because less thermal energy is available. Thus, less infrared radiation is emitted. In the following pictures 7 and 8, it seems that colder areas show up. The dark blue spot in the bottom right indicates a small crack where the PPA-GF30 insert gets pushed out. The negative temperature difference could result due to a macroscopic hole in the specimen that reveals the colder background. The black area at the upper end of the thermogram is a consequence of the movement of the specimen in the tensile testing machine and its impact of the difference image. In addition, contrary to [15], the inversely proportional relation between delamination size and surface temperature could not be verified.

Comparing two consecutive frames of the specimens tested at the two temperatures during a damage event (see Figure 7), it clearly stands out that a strong localized heat contrast occurs suddenly at $23\text{ }^{\circ}\text{C}$, while it occurs slowly and less localized $60\text{ }^{\circ}\text{C}$. This observation coincides with the mechanical data shown in Figure 4c, where on the one hand, sudden damage events are observed at $23\text{ }^{\circ}\text{C}$. On the other hand, the damage mechanism changes to slowly occurring, smooth damage at $60\text{ }^{\circ}\text{C}$.

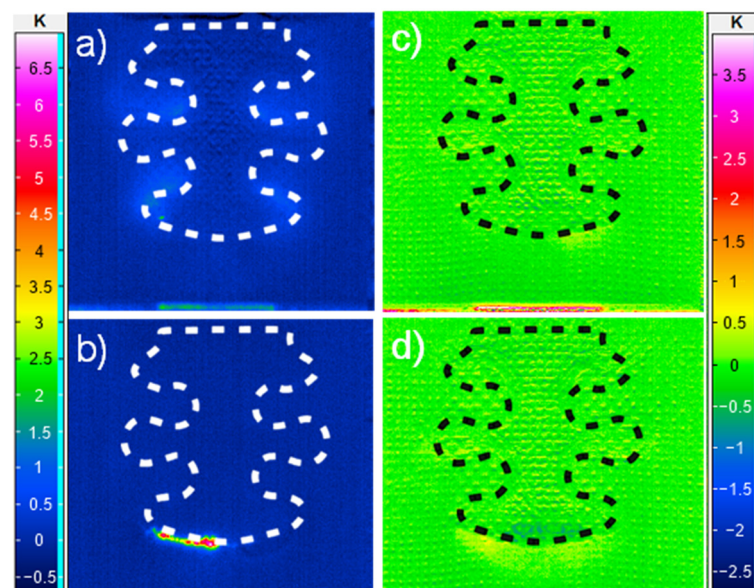


Figure 7. ΔT -thermograms of two consecutive frames (0.33 s time difference) of each temperature during a damage event: (a) first frame $23\text{ }^{\circ}\text{C}$, (b) second frame $23\text{ }^{\circ}\text{C}$, (c) first frame $60\text{ }^{\circ}\text{C}$, (d) second frame $60\text{ }^{\circ}\text{C}$.

Complementary to the thermography images showing all the damage at the surface or near-surface, the X-ray images in Figure 8 unveil the damage on the inside of the hybrid. Compared to the unloaded state a) it can be recognized that the arms of the aluminium insert are bent upwards. This applies for both tested temperatures. At $60\text{ }^{\circ}\text{C}$, the arms are more bent than at $23\text{ }^{\circ}\text{C}$, which is accompanied by the higher deformation. Additionally, the PPA-GF30 part of the insert can be seen in the light grey contrast and is severely damaged. As the aluminium insert is pulled out, the PPA-GF30 breaks partly and releases the insert.

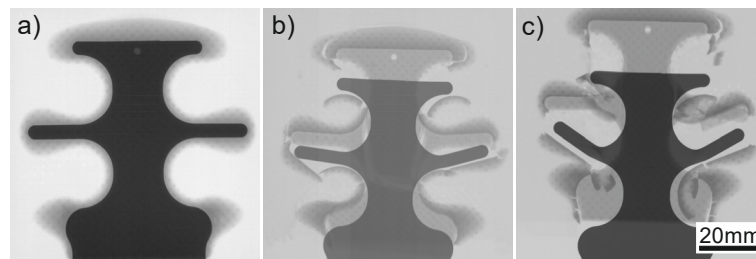


Figure 8. Two-dimensional projections of te hybrid specimens: (a) reference, (b) tested @ 23 °C, and (c) tested @ 60 °C (70 kV acceleration voltage, 49 μm pixel size), respectively.

3.2. Dynamical Testing

In addition to the quasi-static testing, dynamical testing is carried out for all specimen types. The mechanical results are shown in Figure 9 and a comparative analysis is given in Table 3. The dynamical stiffness is plotted against the number of cycles for both temperatures. Moreover, mean values for initial stiffness and cycles to failure are shown in Figure 9d. Looking at Figure 9a, one could assume that there is a significant difference in lifetime of the PPA-GF30 specimens, but the rest of the specimens do not support this hypothesis.

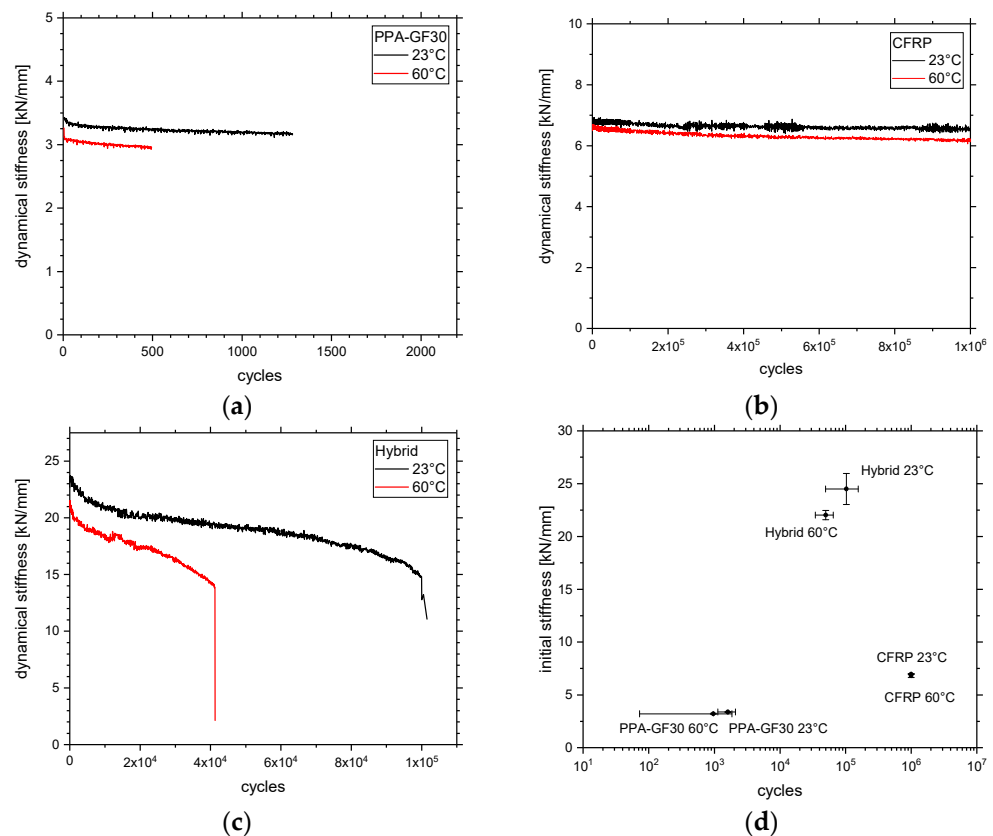


Figure 9. Results from dynamical testing for (a) PPA-GF30, (b) CFRP, and (c) hybrid specimens; (d) mean values of initial stiffness and cycles to failure.

Regarding the PPA-GF30 specimens, it can be noted directly that the number of cycles both specimens withstand is comparably low. There is no evident difference in lifetime between the two temperatures, but there is a small difference in the dynamical stiffness that can be explained due to the viscoelastic behaviour of polymers. The wide error bars of the PPA-GF30 experiments result from the logarithmic representation and the very few

cycles. Furthermore, there is a small linear decrease in mechanical stiffness with increasing cycles for the PPA-GF30 specimens.

Table 3. Comparative analysis at the two different testing temperatures. The stop criterium is 1,000,000 cycles.

Specimen Type	Initial Stiffness [kN/mm]		Cycles	
	23 °C	60 °C	23 °C	60 °C
PPA-GF30	3.38 ± 0.02	3.08 ± 0.2	1607 ± 392	956 ± 728
CFRP	6.79 ± 0.04	6.57 ± 0.09	1,000,000	1,000,000
Hybrid	24.00 ± 1.2	21.34 ± 0.32	103,000 ± 43,778	50,000 ± 12,468

This effect can be observed for the CFRP specimens at both temperatures as well. In addition, there is no failure over the examined one million cycles in CFRP and also a small difference in the initial stiffness. The error bars of the CFRP experiments are minimal in both directions. The scattering in the x-direction is non-existent because all three tests were stopped at one million cycles. This points out the good fatigue performance of the CFRP compared to the other specimen types. The good reproducibility and the well-defined test parameters lead to a small error bar in y-direction.

The temperature shift seems to have the most effect on the hybrids. The initial stiffness at 60 °C is considerably smaller than at 23 °C. The hybrid tested at the higher temperature also seem to withstand a lower number of cycles. Furthermore, the stiffness decreases faster at 60 °C. For both temperatures, three phases of damage can be observed, forming an “S” shaped curve. It first comes to a fast reduction of the dynamical stiffness followed by a smaller linear reduction over the most cycles. In the final stage, the reduction of the dynamical stiffness accelerates again until failure. Looking at the error bars in Figure 9d, different things must be pointed out. To understand these observations, it is necessary to consult the non-destructive testing results in Figure 10.

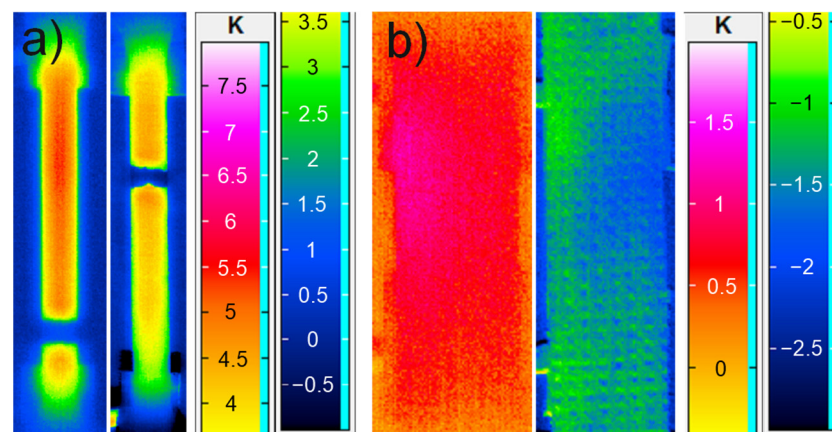


Figure 10. ΔT -thermograms of the (a) PPA-GF30 specimens at 23 °C (left) and 60 °C (right) after failure and (b) CFRP specimens 23 °C (left) and 60 °C (right) after one million cycles in dynamical testing.

First, it can be noted that the PPA-GF30 specimens at both temperatures become noticeably warmer during the short testing period. Differences up to 6 °C in surface temperature can be measured between start of experiment and failure. This strong heating mirrors the high damping in the polymer. It must be considered here that the force-controlled experimental set-up leads to a higher deformation speed with decreasing stiffness compared to CFRP or hybrid specimens. The PPA-GF30 specimens are the least stiff specimens examined here, which means they are tested with the highest deformation speed. Furthermore, the included glass fibre can increase the inner friction and thus the damping. The high damping along with the high deformation speed could also be the reason for the

fast failure occurring at those specimens. Significant differences in the heat up between the specimens tested at 23 °C and 60 °C cannot be observed.

The CFRP specimens show no significant temperature increase during fatigue testing. The marginal difference of ± 1 °C is in the region of day and night fluctuations. This negligible difference can be explained through the fact that the biggest fraction of the load is taken up by the linear elastic carbon fibres and not by the viscoelastic polymer itself. That leads to a lower damping and to a smaller heating. While no failure occurs, no damage events can be identified.

Regarding the thermograms of the hybrid specimens in Figure 11, a heating around the inlay can be observed for all number of cycles at both testing temperatures. The heated-up area grows with rising number of cycles. The temperature of the surrounding CFRP remains unchanged. For both specimens, there is a little stronger heating between the arms of the inlay at first. Subsequently, a hot area emerges below the inlay and shortly before failure there is a strong heating up to 5 °C around the inlay. Significant differences in the fundamental damage mechanisms cannot be detected with this method.

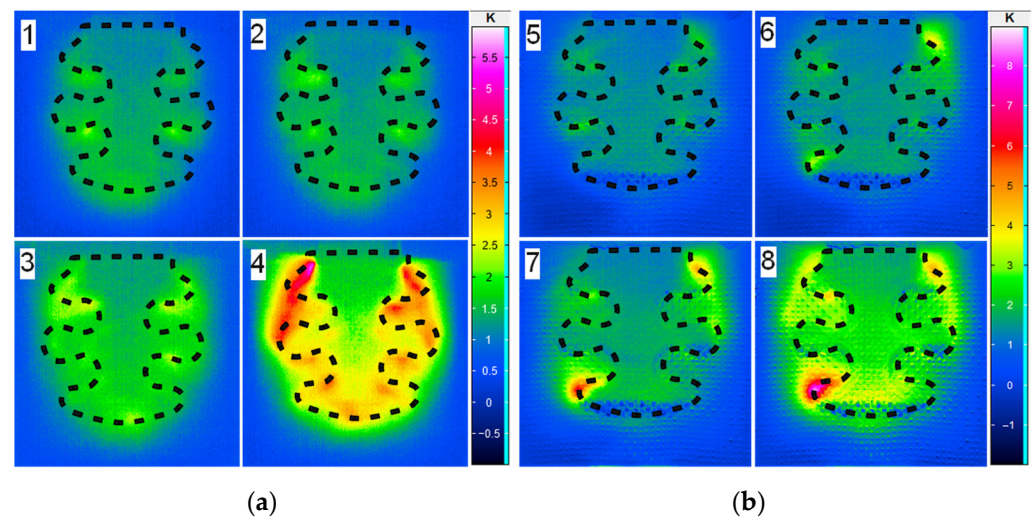


Figure 11. ΔT -thermograms of the hybrid specimens in dynamical testing @ 23 °C (1–4) and 60 °C (5–8); (a) @ 10^4 , 3×10^4 , 6×10^4 , 10^5 cycles; (b) @ 10^4 , 2×10^4 , 3×10^4 , 4×10^4 cycles.

Using Lock-In thermography displaying the phase contrast of thermal waves provides further information about the ongoing damage mechanisms. Delamination growth can be observed in dependence of the number of cycles, and it can be differentiated between delaminated area and delamination front (Figure 12).

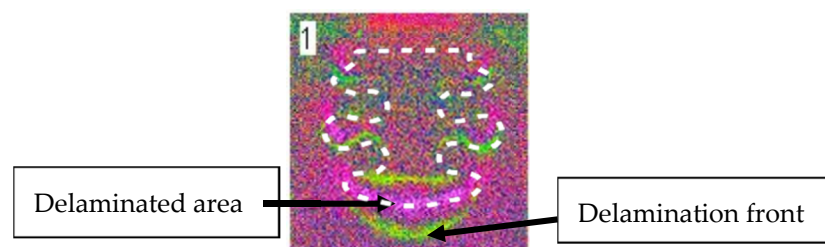


Figure 12. Differentiation between delaminated area and delamination front in Lock-In thermography.

For both testing temperatures, the delamination growth starts below the inlay and between the arms of the inlay (see Figure 13). From these areas, the delaminations enlarge until they grow together to one global delamination, and it comes to failure. A fundamental difference in the damage mechanisms between those two temperatures cannot be detected either.

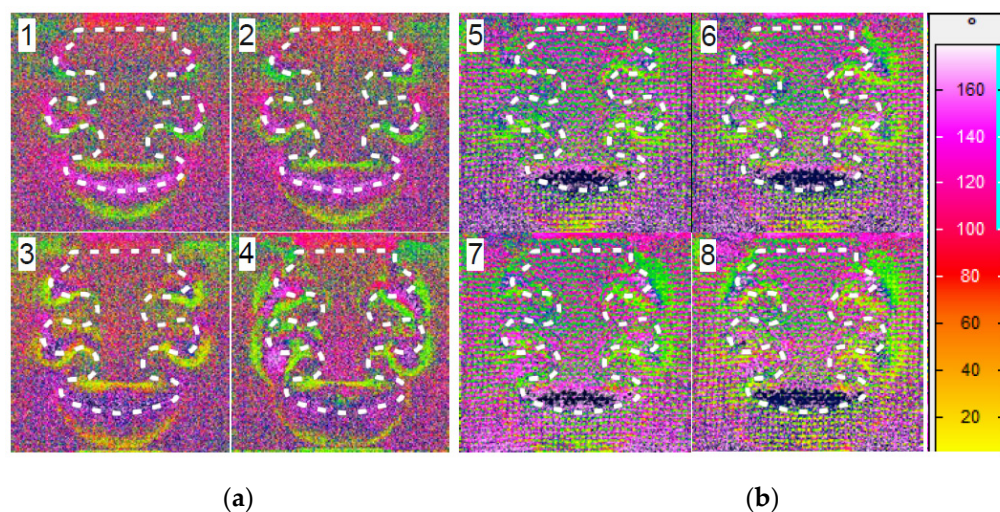


Figure 13. Phase images of the hybrid specimens in dynamical testing @ 23 °C (1–4) and 60 °C (5–8); (a) @ 10^4 , 3×10^4 , 6×10^4 , 10^5 cycles; (b) @ 10^4 , 2×10^4 , 3×10^4 , 4×10^4 cycles.

In contrast to thermography, a significant difference in damage progression can be observed in the X-ray projections (Figure 14) recorded after mechanical testing. While the specimen tested at 23 °C shows a crack in the aluminium inlay, the specimen tested at 60 °C does not show any damage in the aluminium inlay. Both specimens have slightly bent “arms”. Hence, the mechanical data as well as the NDT-data imply an influence of the temperature on the fatigue behaviour of the hybrid.

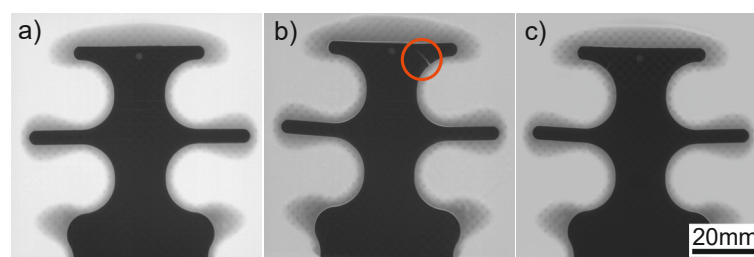


Figure 14. Two-dimensional projections of the hybrid specimens; (a) reference, (b) after dynamical testing @ 23 °C, and (c) @ 60 °C, respectively.

After regarding all the different mechanical, thermographic, and CT data, it has to be analysed why some of them show more temperature effect than others. To conclude this paper, a discussion about the underlying reasons considering the behaviour of the hybrid as well as the influence of the specific single materials is necessary.

4. Discussion

While the results of the isolated experiments shown in the previous section did not always provide an unambiguous result about the influence of the testing temperature, the particular tendencies sum up to a clearer picture.

At quasi-static testing the most obvious difference is the change in damage behaviour of the hybrid that can be regarded in the force displacement diagram and in the thermograms as well. While the specimens at room temperature break in short, abrupt damage events, the heated ones fail without those events and in a smoother curve after lasting a higher displacement. Looking at two subsequent thermograms, clear and concrete areas in which abrupt damage events take place can be identified, whereas at 60 °C no suddenly emerging damage can be observed. On the other hand, the specimens of the single materials (CFRP and PPA-GF30) break at similar displacements with the same damage behaviour

respectively for both temperatures. The heated specimens endure a slightly lower force and maintain a lower Young's modulus.

This leads to the assumption that the elevated temperature primarily effects the interfaces in the hybrid specimen. The reason could be a premature debonding of CFRP like it is described in [21]. A possible reason for this debonding could be residual stresses caused by different thermal expansion coefficients of the three single materials. Such effects are described in [23]. This would not necessarily affect the overall performance of the hybrid too much due to the geometrical interlocking of the inlay and it would explain the absence of the abrupt damage events. Another assumption under these observations is a softening of the single materials in the hybrid at elevated temperatures leading to a reduction of locally concentrated interfacial tension during experiments due to higher polymer mobility. Higher local tensions can lead to a localized damage event, even if the global tension to initiate the component failure is not reached yet. A local damage like this would weaken the specimen as a whole and lead to tensions on other places and thus to a damage cascade as observed in Figure 4c. This is also evidenced by the local, sudden temperature peaks which only occur at 23 °C corresponding to an abrupt unloading of these localized tensions. The CT-projections after quasi-static testing cannot deliver further information to support or contradict this hypothesis.

Looking at the dynamical experiments with regard to the observations made in quasi-static testing a few more things stand out. Firstly, there is a reduction in life cycles as well as in the initial stiffness for the 60 °C hybrid specimens. The single-material specimens, in contrast, only show a small difference in their mechanical behaviour at the two tested temperatures. This fact points to the influence of the temperature on the interfaces.

Thermography does not show differences in the damage mechanisms in dynamical testing between the two temperatures. However, the CT-projections after dynamical testing support the local tension hypothesis from the quasi-static experiments. The cracks in aluminium occurring in the hybrid specimens at 23 °C can also be explained due to high local tensions that lead to fatigue crack growth in the metal. Ostermann [14] suggests that this happens due to dislocation gliding which is the predominant deforming mechanism in aluminium. The absence of these cracks at 60 °C on the other hand shows that a softening of the polymers may reduce those tensions.

Summarizing the effects, the mechanical behaviour of a metal–CFRP hybrid structure under quasi-static and dynamic load changes at elevated temperature. The switch of damage mechanisms occurs at temperature differences, which a component out of these materials could be exposed to in daily life use.

These observations suit those published in [21–23]. Despite different material combinations and specimen designs, a change in damage mechanisms and a decrease in mechanical properties at elevated temperatures happen for all tested CFRP–metal hybrids. The initial hypothesis of testing the single components and therefrom extrapolating to the hybrid properties and behaviour could not be applied as intended. However, it turns out that the behaviour of the hybrid is more than the sum of its single materials.

As an overall result it can be concluded that the knowledge about the mechanical properties under different thermal conditions of the including materials is not sufficient to understand the behaviour of a hybrid under those condition as a whole, because the interface behaviour plays a major role as well.

5. Conclusions and Outlook

- In the quasistatic experiments, the elevated temperature (60 °C) leads to a small decrease in the sustained maximum force of the single material without affecting the sustained maximum force of the hybrid specimen significantly. Nonetheless, a difference in occurring damage is observed for the hybrid. While there are abrupt damage events at 23 °C, there is a smoother damage progression at 60 °C, which goes along with a significant increase in displacement at failure for the elevated temperature.

- In the dynamic experiments, the initial dynamical stiffness of all specimen types decreases at elevated temperatures. The sustained cycles of PPA-GF30 and hybrid specimens decrease as well. The elevated temperature worsens the overall fatigue performance of the hybrid significantly.
- The used nondestructive testing techniques support the observations of the mechanical testing and give further information about the underlying damage mechanisms. The abrupt damage events can also be seen and localized in thermography. By using CT, occurring damage in the metal inlay at lower temperatures can be observed.
- The investigated hybrid specimen is a complex system containing of three single materials with two interfaces and interlockings. A temperature change affecting one part of the system has an influence on other parts and change the damage mechanism in a hard-to-calculate way.

Further investigations including the role of the interface, hybrid samples of different geometries, and more temperature levels must be analysed to obtain a deeper look. The question of whether the transition of the damage mechanism happens at a specific temperature or over a wider temperature range is also not answered yet. Moreover, the influence of further external influences, i.e., humidity should be monitored as well. A shortcoming in this work is the missing observation of the isolated interfaces in a simpler geometry (i.e., single lap joints). Such an investigation could give a deeper understanding of what exactly happens at the interfaces.

Author Contributions: Investigation, F.G., H.J.; Writing—original draft, H.J., F.G.; Writing—review & editing, H.-G.H. All authors have read and agreed to the published version of the manuscript.

Funding: This research was funded by DFG (Deutsche Forschungsgemeinschaft) project number 237091934.

Acknowledgments: We acknowledge support by the Deutsche Forschungsgemeinschaft (DFG, German Research Foundation) and Saarland University within the funding programme Open Access Publishing. The authors kindly thank their research associates from WBK institute at KIT, LKT at TU Dortmund, as well as the German research committee for the project funding.

Conflicts of Interest: The authors declare no conflict of interest.

References

1. Delogu, M.; Zanchi, L.; Dattilo, C.A.; Pierini, M. Innovative composites and hybrid materials for electric vehicles lightweight design in a sustainability perspective. *Mater. Today Commun.* **2017**, *13*, 192–209. [[CrossRef](#)]
2. Meschut, G.; Janzen, V.; Olfermann, T. Innovative and Highly Productive Joining Technologies for Multi-Material Lightweight Car Body Structures. *J. Mater. Eng. Perform.* **2014**, *23*, 1515–1523. [[CrossRef](#)]
3. Summa, J. In Situ Thermographie Zur Prognose Des Ermüdungsrisswachstums in Intrinsischen Al-CFK Hybridbauteilen Unter Zugschwellender Ermüdung Im High-Cycle Regime. Ph.D. Thesis, Saarland University, Saarbrücken, Germany.
4. Schwarz, M.; Schwarz, M.; Herter, S.; Herrmann, H.-G. Nondestructive Testing of a Complex Aluminium-CFRP Hybrid Structure with EMAT and Thermography. *J. Nondestruct. Eval.* **2019**, *38*, 35. [[CrossRef](#)]
5. Schwarz, M. Multimodale zerstörungsfreie Charakterisierung der Grenzflächen von Metall-CFK-Hybridstrukturen. Ph.D. Thesis, Saarland University, Saarbrücken, Germany, 2019.
6. Summa, J.; Becker, M.; Grossmann, F.; Pohl, M.; Stommel, M.; Herrmann, H.-G. Fracture analysis of a metal to CFRP hybrid with thermoplastic interlayers for interfacial stress relaxation using in situ thermography. *Compos. Struct.* **2018**, *193*, 19–28. [[CrossRef](#)]
7. Schwarz, M.; Summa, J.; Quirin, S.; Herrmann, H.G. New Approaches in Nondestructive Characterisation of Defects in Metal-CFRP Hybrids. *Mater. Sci. Forum* **2015**, 825–826, 976–982. [[CrossRef](#)]
8. Ucsnik, S.; Scheerer, M.; Zaremba, S.; Pahr, D.H. Experimental investigation of a novel hybrid metal–composite joining technology. *Compos. Part A Appl. Sci. Manuf.* **2010**, *41*, 369–374. [[CrossRef](#)]
9. Jung, K.W.; Kawahito, Y.; Takahashi, M.; Katayama, S. Laser direct joining of carbon fiber reinforced plastic to zinc-coated steel. *Mater. Des.* **2013**, *47*, 179–188. [[CrossRef](#)]
10. Fleischer, J. *Intrinsische Hybridverbunde Für Leichtbautragstrukturen: Grundlagen der Fertigung, Charakterisierung und Auslegung*; Springer: Berlin/Heidelberg, Germany, 2021; ISBN 978-3-662-62832-4.
11. Fleischer, J.; Nieschlag, J. Introduction to CFRP-metal hybrids for lightweight structures. *Prod. Eng.* **2018**, *12*, 109–111. [[CrossRef](#)]
12. Nieschlag, J.; Ruhland, P.; Daubner, S.; Koch, S.-F.; Fleischer, J. Finite element optimisation for rotational moulding with a core to manufacture intrinsic hybrid FRP metal pipes. *Prod. Eng.* **2018**, *12*, 239–247. [[CrossRef](#)]

13. Serna, J.; Zinn, C.; Scharf, I.; Dittes, A.; Schwoebel, S.-D.; Schmidt, C.; Meiners, D.; Schaper, M.; Lampke, T. Concepts for interface engineering and characterization in composite hybrid structures. *IOP Conf. Ser. Mater. Sci. Eng.* **2019**, *480*, 12014. [[CrossRef](#)]
14. Ostermann, F. *Anwendungstechnologie Aluminium*; Springer: Berlin/Heidelberg, Germany, 2014; ISBN 978-3-662-43807-7.
15. Cao, S.; WU, Z.; Wang, X. Tensile Properties of CFRP and Hybrid FRP Composites at Elevated Temperatures. *J. Compos. Mater.* **2009**, *43*, 315–330. [[CrossRef](#)]
16. Im, K.-H.; Cha, C.-S.; Kim, S.-K.; Yang, I.-Y. Effects of temperature on impact damages in CFRP composite laminates. *Compos. Part B Eng.* **2001**, *32*, 669–682. [[CrossRef](#)]
17. Miyano, Y.; Nakada, M.; Kudoh, H.; Muki, R. Prediction of tensile fatigue life under temperature environment for unidirectional CFRP. *Adv. Compos. Mater.* **1999**, *8*, 235–246. [[CrossRef](#)]
18. Domininghaus, H.; Elsner, P.; Eyerer, P.; Hirth, T. *Kunststoffe: Eigenschaften Und Anwendungen*; 8., neu bearb. und erw. Aufl.; Springer: Berlin/Heidelberg, Germany, 2012; ISBN 978-3-642-16173-5.
19. Lyons, J.S. Time and temperature effects on the mechanical properties of glass-filled amide-based thermoplastics. *Polym. Test.* **1998**, *17*, 237–245. [[CrossRef](#)]
20. Lyons, J.S.; Tinio, E.G.; Berry, S.F. Creep, stress rupture, and isothermal aging of reinforced polyphthalamide. *J. Appl. Polym. Sci.* **1995**, *56*, 1169–1177. [[CrossRef](#)]
21. Ke, L.; Li, C.; He, J.; Shen, Q.; Liu, Y.; Jiao, Y. Enhancing fatigue performance of damaged metallic structures by bonded CFRP patches considering temperature effects. *Mater. Des.* **2020**, *192*, 108731. [[CrossRef](#)]
22. Chen, Y.; Yang, X.; Li, M.; Mei, M. Influence of working temperatures on mechanical behavior of hybrid joints with carbon fiber reinforced plastic/aluminum lightweight materials for automotive structure. *J. Manuf. Process.* **2019**, *45*, 392–407. [[CrossRef](#)]
23. Mrzljak, S.; Schmidt, S.; Kohl, A.; Hülsbusch, D.; Hausmann, J.; Walther, F. Testing Procedure for Fatigue Characterization of Steel-CFRP Hybrid Laminate Considering Material Dependent Self-Heating. *Materials* **2021**, *14*, 3394. [[CrossRef](#)] [[PubMed](#)]
24. T300/FT300; Commercial Documentation. Toray Carbon Fibers Europe: Abidos, France, 2012. Available online: <https://toray-cfe.com/wp-content/uploads/2020/12/toray-torayca-t300ft300-haute-resistance.pdf> (accessed on 7 December 2022).
25. Biresin CR170 Mit Biresin CH150-3 Härter; Data Sheet; Sika: Bad Urach, Germany, September 2020. Available online: https://industry.sika.com/dms/getdocument.get/ed43cb3a-98e6-49e1-b396-cfae053f7610/Biresin_CR170-CH150-3-New.pdf (accessed on 7 December 2022).
26. AlMgSi1 EN AW-6082; Data Sheet; Schmolz + Bickenbach: Krefeld, Germany, March 2011. Available online: <https://pdf4pro.com/view/3-2315-almgsi1-alsimgmn-en-aw-6082-1b7af2.html> (accessed on 7 December 2022).
27. VESTAMID HTplus M1033-PA66/6T-GF30; Data Sheet. Evonik: Essen, Germany, 2018. Available online: <http://www.campusplastics.com/> (accessed on 11 September 2018).
28. DIN EN ISO 527-4; DIN. Plastics-Determination of Tensile Properties-Part 4: Test Conditions for Isotropic and Orthotropic Fibre-Reinforced Plastic Composites. Beuth Verlag: Berlin, Germany, 2020.
29. DIN EN ISO 527-2; DIN. Plastics-Determination of Tensile Properties-Part 2: Test Conditions for Moulding and Extrusion Plastics. Beuth Verlag: Berlin, Germany, 2012.
30. Rösner, H.; Netzelmann, U.; Hoffmann, J.; Karpen, W.; Kramb, V.; Meyendorf, N. Thermographic Materials Characterization. In *Nondestructive Materials Characterization*; Hull, R., Osgood, R.M., Parisi, J., Warlimont, H., Meyendorf, N.G.H., Nagy, P.B., Rokhlin, S.I., Eds.; Springer: Berlin/Heidelberg, Germany, 2004; pp. 246–285; ISBN 978-3-642-07350-2.
31. Maldague, X.P.V. *Theory and Practice of Infrared Technology for Nondestructive Testing*; Wiley: New York, NY, USA, 2001; ISBN 978-0-471-18190-3.
32. Meschede, D. *Gerthsen Physik*; 25. Aufl.; Springer: Berlin/Heidelberg, Germany, 2015; ISBN 978-3-662-45977-5.
33. Wu, D.; Busse, G. Lock-In Thermography for Nondestructive Evaluation of Materials. *Rev. Générale Therm.* **1998**, *37*, 693–703. [[CrossRef](#)]
34. Carmignato, S.; Dewulf, W. *Industrial X-ray Computed Tomography*; Springer: Berlin/Heidelberg, Germany, 2018; ISBN 978-3-319-59571-9.
35. InfraTec. *VarioCAM HD Head*; User Manual; InfraTec: Dresden, Germany, 2012.